Quantum Dynamical Averaging Over an Ensemble of Molecular Orientations by a Singular Value Decomposition of the Density Matrix

Manuel Cardosa Gutierrez[1], R. D. Levine[2,3,4], F. Remacle[1,2*]

[1]Theoretical Physical Chemistry, UR MOLSYS, University of Liege, Belgium
[2]Fritz Haber Center, Institute of Chemistry, The Hebrew University of Jerusalem, Jerusalem 91904, Israel
[3] Department of Molecular and Medical Pharmacology, David Geffen School of Medicine
and
[4] Department of Chemistry and Biochemistry, University of California, Los Angeles, CA 90095, USA

We report a robust and compact methodology for averaging quantum photoexcitation dynamics over the initial orientations of the molecules with respect to an ultrashort light pulse. We use singular value decomposition of the density matrix of the excited molecules which allows identifying the few dominant principal molecular orientations with respect to the polarization direction of the electric field. The massive compaction of the density matrix of the ensemble of randomly oriented pumped molecules enables a most efficient fully quantum mechanical time propagation scheme. Two examples are discussed for the quantum dynamics of the LiH molecule in the manifolds of its electronically excited Σ and Π states.

*Corresponding author: F. Remacle, fremacle@uliege.be

Introduction

Recent progress in attoscience[1-2] open the way to new avenues for controlling chemical reactivity through the selective excitation of a superposition of electronic states with the short-in-time-broad-in-energy attopulse.[3] As pointed out very early,[4] the orientation of the molecule with respect to the polarization direction of the pulse electric field is a very effective way to control the initial superposition built by the pulse and therefore the subsequent dynamics. Molecules can be oriented using a single or a sequence of laser pulses, enabling to carry out field free photoexcitation or photoionization experiments in the molecular frame. [5-9] However, the achievable orientation is typically limited to values of $\langle \cos\theta \rangle \approx 0.7$ and $\langle \cos^2\theta \rangle \approx 0.8$. Moreover, the proposed experimental approaches to orient molecules are not applicable to all types of molecules.[10-12] Therefore, it is often the case that a realistic description of quantum dynamics of molecules photoexcited by short atto and few fs pulses requires an averaging over the molecular orientations with respect to the polarization direction of the exciting optical pulse. However, averaging quantum dynamics simulations over an ensemble of molecular orientations can be computationally rather costly in computer time and storage capacity since the quantum dynamical propagation needs to be repeated as many times as the number of molecular orientations in the ensemble. While such an orientation averaging is manageable computationally for diatomic molecules, it becomes out of reach for quantum dynamical simulation involving several nuclear degrees of freedom on coupled electronic states, as typical when molecules and molecular cations are excited by ultrashort, broad in energy atto pulses.[2, 13] Here we propose a numerical approach for computing the ensemble dynamics of randomly oriented molecules interacting with an ultrashort optical pulse that considerably lowers the computational resources and provides insights on the orientation effects. Our approach is based on the Singular Value Decomposition (SVD)[14] of the matrix built from the pure quantum states associated with each molecular orientation of the ensemble. This matrix, **A**, is a rectangular matrix with dimension, N_b, the number of basis set functions used to expand the wave function, times the number of molecular orientations, N_o. Typically, after the pulse is over, only a few principal components suffice to obtain an accurate description of the matrix **A**. The SVD principal components identify the most important orientations that contribute to the ensemble dynamics (the singular orientation vectors) and the corresponding molecular pure quantum states (the singular molecular states). In addition to provide physical insights on the role of orientation averaging on the ensemble dynamics, we show that the SVD compaction significantly reduces the cost of computing the quantum dynamics of the ensemble since only

few singular (pure) quantum states need to be stored and propagated after the pulse to accurately describe the ensemble quantum dynamics. An exact description is obtained by retaining as the number of principal components the smallest dimension of **A** matrix, which is typically the number of orientations, N_o. For an approximate description, one can adjust the number of retained principal components necessary to reach a specified accuracy threshold. We find that only a few components are required for a satisfactory semi-quantitative description

SVD approach to quantum dynamics averaged over random orientations

At time $t = 0$, the molecules of the ensemble are in their ground electronic state. The different molecules of the ensemble are distributed over their particular orientation, o, with respect to the polarization direction of the exciting pulse. Each initial orientation, o, at the time before excitation defines a pure state, $\left|\Psi_o\left(t=0\right)\right\rangle$. During and after the excitation by the atto pulse each initial state evolves into $\left|\Psi_o\left(t\right)\right\rangle$, a coherent combination represented as a Born-Huang expansion, a sum of N_b separable terms in the nuclear and electronic degrees of freedom:

$$\left|\Psi_o\left(t\right)\right\rangle = \sum_{b=1}^{Nb} c_b^o\left(t\right)\left|b\right\rangle \qquad (1)$$

where $c_b^o\left(t\right)$ is the Born-Huang amplitude of the vibronic basis function $\left|b\right\rangle$ for the initial orientation, o. The index b stands for a nuclear and an electronic index which, for a pulse broad in energy, includes several coupled electronic states. In general we expect that the number of terms in Eq. (1) is such that $N_b >> N_o$, where N_o is the number of molecular orientations in the ensemble. The amplitudes $c_b^o(t)$ are computed by integrating the Time-Dependent Schrödinger Equation (TDSE), on a basis of N_g grid functions for the nuclear coordinates for N_e coupled adiabatic electronic states, which leads to $N_b = N_g$ x N_e:

$$i\hbar\frac{d\mathbf{c}_o}{dt} = \mathbf{H}\mathbf{c}_o \qquad (2)$$

The inequality $N_b >> N_o$ is primarily because the number N_g of grid points needs to be large. The molecular Hamiltonian, **H**, includes the coupling to the electric field of the pulse, $\mathbf{E}\left(t\right)$, in the dipole approximation and the non adiabatic coupling (NAC) between the electronic states driven by the nuclear motion. For a diatomic molecule,

$$\mathbf{H} = -\frac{1}{2\mu}\left(\nabla_R^2 + 2\boldsymbol{\tau}\left(R\right).\nabla_R + \left(\nabla_R\boldsymbol{\tau}\left(R\right)\right) + \boldsymbol{\tau}\left(R\right).\boldsymbol{\tau}\left(R\right)\right) + \mathbf{V}\left(R\right) - \mathbf{E}\left(t\right).\boldsymbol{\mu} \qquad (3)$$

In Eq. (3), the second and third terms are the NAC terms and $\mathbf{V}(R)$ the potential term. The last term is the dipole coupling, where the orientation of the electric field vector, $\mathbf{E}(t)$, is defined in the molecular frame attached to the center of mass of the molecule. This considerably simplifies the numerical integration and is equivalent to defining the orientation of the molecular frame with respect to the orientation of the electric field in the laboratory frame. Note that one needs to rotate back to the laboratory frame before analyzing angular distributions.

During the pulse, the Hamiltonian depends on time. One needs to take into account the orientation of the electric field with respect to the molecule to describe the excitation dynamics. We do so by integrating the TDSE during the pulse for all the N_o orientations of $\mathbf{E}(t)$, each computed separately, obtaining N_o time-dependent pure states $\left|\Psi_o(t)\right\rangle$. These states are gathered into a rectangular, complex, N_b x N_o, matrix $\mathbf{A}$ with typically $N_o < N_b$. Singular Value Decomposition (SVD) provides an exact description of the matrix $\mathbf{A}$ as a sum of a maximum of N_o separable terms, its principal components.[14] The SVD factorization of $\mathbf{A}$ is a sum of direct products of a left, $\mathbf{U}_m$, and a right, $\mathbf{V}_m^\dagger$, singular complex eigenvector weighted by the corresponding (real) singular value, σ_m,

$$\mathbf{A}(t) = \sum_{m=1}^{N_o} \sigma_m(t)\, \mathbf{U}_m(t) \otimes \mathbf{V}_m^\dagger(t) \qquad (4)$$

In each principal component, m, the right singular vector, $\mathbf{V}_m(t)$, has N_o components, $v_{om}(t)$, and depends only on the orientation index, o, and the left singular vector, $\mathbf{U}_m(t)$, has N_b components, u_{bm}, and depends only on the basis set index b. Throughout, we refer to $\mathbf{V}_m(t)$ as the orientation singular vector and to $\mathbf{U}_m(t)$ as the molecular singular vector.

From the rectangular $\mathbf{A}$ matrix, one can construct two reduced square density matrices. The N_b x N_b density matrix of the ensemble of molecules, $\rho_{mol}(t)$, is the trace over the orientations and depends on the molecular degrees of freedom only. It is the $\mathbf{AA}^\dagger$ quadratic form of the matrix $\mathbf{A}(t)$: [15],

$$\rho_{mol}(t) = (1/N_o)\mathbf{A}\mathbf{A}^\dagger = (1/N_o)\sum_{o=1}^{N_o} \mathbf{c}_o(t)\mathbf{c}_o^\dagger(t) = (1/N_o)\sum_{b=1}^{N_b}\sum_{b'=1}^{N_b} |b\rangle\left(\sum_{o=1}^{N_o} c_b^o(t)c_{b'}^{o'}(t)\right)\langle b'| \qquad (5)$$

Inserting Eq. (4) into Eq. (5), one gets

$$\rho_{mol}(t) = (1/N_o)\sum_{m,m'} \sigma_m(t)\sigma_{m'}(t)\left(\mathbf{U}_m \otimes \mathbf{V}_m^{\dagger}\right).\left(\mathbf{V}_{m'} \otimes \mathbf{U}_{m'}^{\dagger}\right)$$
$$= (1/N_o)\sum_{m,m'} \sigma_m(t)\sigma_{m'}(t)\left(\mathbf{U}_m \otimes \left(\mathbf{V}_m^{\dagger}.\mathbf{V}_{m'}\right) \otimes \mathbf{U}_{m'}^{\dagger}\right) \qquad (6)$$
$$= (1/N_o)\sum_{m} \sigma_m^2(t)\left(\mathbf{U}_m \otimes \mathbf{U}_m^{\dagger}\right)$$

where the last line is obtained by taking into account the orthogonality of the orientation singular vectors so that $\mathbf{V}_m^{\dagger}\mathbf{V}_{m'} = \delta_{mm'}$. $\rho_{mol}(t)$ depends on the singular molecular vectors only. Similarly, one can define the complementary N_o x N_o reduced density matrix, $\rho_{orient}(t)$, by the quadratic form $\mathbf{A}^{\dagger}\mathbf{A}$:

$$\rho_{orien}(t) = (1/N_o)\sum_{m,m'} \sigma_m(t)\sigma_{m'}(t)\left(\mathbf{V}_m \otimes \mathbf{U}_m^{\dagger}\right).\left(\mathbf{U}_{m'} \otimes \mathbf{V}_{m'}^{\dagger}\right)$$
$$= (1/N_o)\sum_{m,m'} \sigma_m(t)\sigma_{m'}(t)\left(\mathbf{V}_m \otimes \left(\mathbf{U}_m^{\dagger}.\mathbf{U}_{m'}\right) \otimes \mathbf{V}_{m'}^{\dagger}\right) \qquad (7)$$
$$= (1/N_o)\sum_{m} \sigma_m^2(t)\left(\mathbf{V}_m \otimes \mathbf{V}_m^{\dagger}\right)$$

which depends on the orientation singular vectors only.

During the pulse, the electronic and nuclear degrees of freedom are coupled to the orientations through the dipole terms, which leads to a time dependence of the singular values $\sigma_m(t)$. When the pulse is over, the dipole coupling terms vanish and the Hamiltonian, Eq. (3), becomes stationary. Then the singular values become stationary since we consider a non rotating molecule. Note that the two partial traces have the same set of eigenvalues, which are the square of the singular values, σ_m, of **A**:

$$\mathrm{Tr}\left[\rho_{mol}(t)\right] = \mathrm{Tr}\left[\rho_{orien}(t)\right] = \left(\frac{1}{N_o}\right)\sum_{m=1}^{N_o} \sigma_m^2(t) = 1. \qquad (8)$$

with $\sum_{m-1}^{N_o}\sigma_m^2(t) = N_o$. The SVD of the **A** matrix at the end of the pulse, at time t_i, therefore provides a set of orthogonal pure states, $\mathbf{U}_m$, that each corresponds to a specific singular orientation of the molecule as defined by the corresponding orientation singular vector $\mathbf{V}_m$. We show below that only a few singular values $\sigma_m(t_i)$, $N_{\min} \le N_o$, suffice to recover accurately the molecular density matrix, $\rho_{mol}(t_i)$, at the end of the pulse. One can set a maximum number of singular values needed by putting a threshold on how well the norm is recovered:

$$\Delta_{N\min} = 1 - \mathrm{Tr}\left[\rho_{mol}^{N\min}(t_i)\right] = 1 - \left(\frac{1}{N_o}\right)\sum_{m=1}^{N\min} \sigma_m^2(t_i) \geq 0 \qquad (9)$$

Since the molecular Hamiltonian is stationary after the pulse and the molecule is not rotating, the singular values are stationary as well. One can therefore set up a very efficient propagation scheme for the density matrix of the ensemble of molecules after the pulse is over by only propagating with the molecular Hamiltonian (Eq. (3)) the few, $N\min$, $\mathbf{U}_m$ vectors that correspond to the largest singular values:

$$i\hbar\, d\mathbf{U}_m / dt = \mathbf{H}\mathbf{U}_m \text{ for } t > t_i, \text{ with } \mathbf{U}_m(t_i) = \sum_{b=1}^{b} u_{bm}(t_i)\left|b\right\rangle \qquad (10)$$

where the initial values, $u_{bm}(t_i)$, are the coefficients of the $\mathbf{U}_m$ vectors at the time t_i (the end of the pulse).

Providing that the TDSE is integrated accurately so that the integration error is smaller that $\Delta_{N\min}$, the numerical error, Eq. (9), that is due to the fact that we use a restricted number of principal components of the matrix **A,** does not increase with time. Using Eq. (6), we get

$$\begin{aligned}\rho_{mol}^{N\min}(t) &= (1/N_o)\sum_{m=1}^{N_{\min}}\sigma_m^2(t_i)\sum_{b}^{Nb}\sum_{b'}^{Nb'} u_{bm}^*(t)u_{b'm}^*(t)\left|b\right\rangle\left\langle b'\right| \qquad t > t_i \\ &= (1/N_o)\sum_{m=1}^{N\min}\sigma_m^2(t_i)\rho_m(t)\end{aligned} \qquad (11)$$

To summarize, our approach requires to propagate all the initial states defined by a sampling of the molecular orientations until the pulse is over. Since we consider excitation by short atto or few fs pulses, this propagation time is short, of the order of 20 fs for a pulse with a FWHM of 2 fs. Then when the Hamiltonian is stationary, one performs an SVD analysis of the matrix **A** (Eq. (4)) and retains the $N_{\min}$ largest principal components necessary to reach a specified accuracy threshold. Only these fewer components need to be propagated after the pulse using the TDSE as long as the molecular Hamiltonian remains stationary. This approach reduces the computer time needed to compute quantum molecular dynamics averaged over molecular orientations by at least 2 orders of magnitude for the dynamics of diatomic molecule taking place on several electronic states. The gain is even larger when molecule has several nuclear degrees of freedom. It is also storage efficient because it allows compacting the information of dynamics of the randomly oriented initial states into a few singular components. Using our approach, one does not need to store and analyze the dynamics of the all the randomly orientated initial states.

Results and discussion

We apply our scheme to the non rotating LiH molecule excited by two deep UV few cycles pulses of different frequency and with the same FWHM of 2 fs (FWHM bandwidth of 1. 82 eV). In the Franck-Condon (FC) region, R_{eq} = 1.6Å (see Figure S2), the transition dipole moment from the GS to the lowest Σ state, Σ_1, along z is smaller than the transition dipole along x or y to the lowest Π state, Π_1, and to the higher Σ and Π states. We report on the dynamics induced using pulses with two different carrier frequencies, ω_0, tuned to access different combinations of Σ and Π states. The first pulse has a carrier frequency of 4.35 eV, so that both the lowest Σ_1 and Π_1 states fall within the pulse energy bandwidth. However, because of the difference in the transition dipole moments, for random orientations, it is the Π_1 state that is accessed, with only very low populations in the Σ_1 and in the entire Σ manifold. The second pulse has a higher carrier frequency of 5.17 eV which allows accessing the higher Σ and Π states with similar probabilities. The strength of the electric field is 0.01 a.u. (3.51 10^{12} W/cm^2).

The dynamics induced by the first pulse is used for benchmarking the SVD approach for random initial molecular orientations. Excitation by the 4.35 eV pulse yields very different populations: the population of the Π_1 state is 1-2 orders of magnitude larger than that of the Σ states. To benchmark our approach, we computed the time evolution by solving the TDSE for 800 random initial orientations using Eq. (2). The electronic structure parameters (potential energy, NAC and transition dipole curves) are those reported in ref. [16] and plotted in the SI (figures S1, S2 and S3). The NAC terms couple electronic states of the same symmetry, Σ or Π. Electric fields oriented along the molecular axis (the *z* axis in the molecular frame) can only accessed excited Σ states since the ground state is of Σ symmetry. However, as soon as the electric field has components along x or y in the molecular frame, a linear combination of Σ and Π states is excited. Since the transition dipole to the Π_1 state is larger than to the Σ states and to the other Π states, the averaged populations in the two components of the Π_1 state are much larger than that of the other states. The populations in the electronic states averaged over 800 random molecular orientations are plotted in figure 1a for the Π_1 state and in figure 1b for the Σ manifold and the Π_2 state.

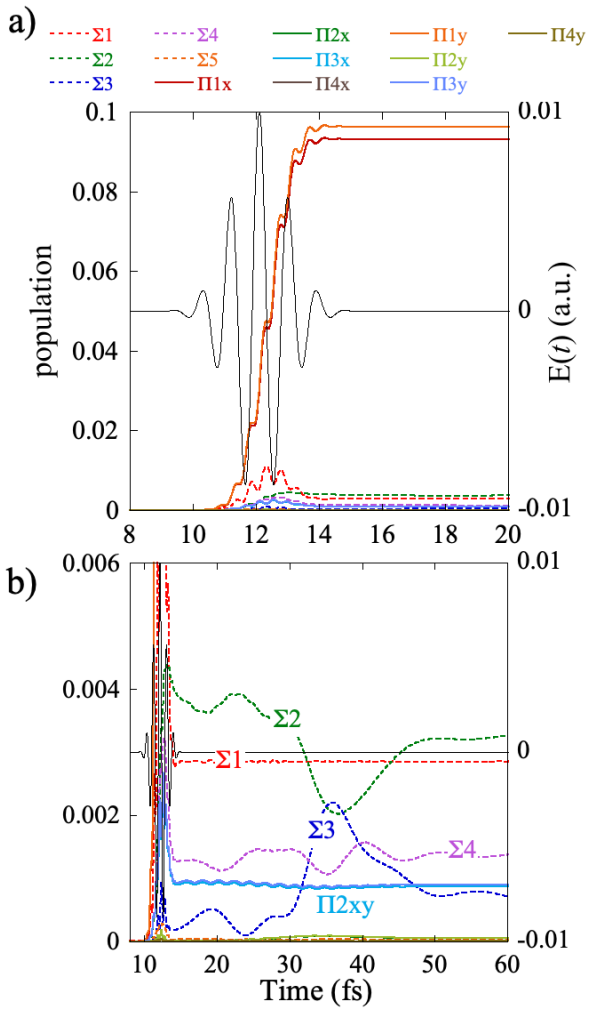

Figure 1. Populations averaged over 800 molecular orientations in the Π_1 state (a) and (b) in the Σ manifold (Σ_2, Σ_3 and Σ_4) and the Π_2 states computed for an excitation by the deep UV 2fs pulse of 4.35 eV. The reason why the two components of the Π_1 state are not exactly equal is due to the fact that only 800 orientations are included in the averaging procedure. After the pulse, the population of the Π_1 state is essentially stationnary. The long time behavior is given in Figure S4.

The electronic states within each manifold are coupled by the NAC terms. As can be seen from Fig 1b, the population transfers are far larger within the states of the Σ manifold than for the Π ones. This is mainly due to the fact that the energy difference between the two Π states is much larger, see Figure S4 for the long time behavior of the population in the Π_1 state. For the same reason, the population transfers between the Σ_1 state and the higher Σ states are also small.

Our SVD approach to the ensemble dynamics begins by building the matrix **A** (Eq. (4)) from the 800 randomly oriented $\mathbf{c_o}$ vectors and compute its principal components by SVD at every time step during the excitation by the pulse. The singular values are arranged in order of decreasing magnitude with σ_1 being the largest. The square of the 8 largest singular values, σ_m^2 normalized by N_o the number of initial random orientations are plotted in Fig. 2a as a function of time on a log scale to emphasize how far they decrease in magnitude with increasing order *m*. As discussed above, after the pulse, the Hamiltonian is stationary and the singular values are constant in time. The normalized singular value σ_1 is unity before excitation and remains close to one after the pulse. It can be correlated with the ground electronic state as we discuss below (Figure 4). σ_2 and σ_3 are degenerate during and after the pulse, while σ_6 and σ_7 that are degenerate during the pulse while after the pulse, it is the pair σ_7, σ_8 that are equal. As shown in figure 4 below, these two pairs of singular values are localized on the two Π states, Π_1 and Π_2. One can also see in Figure 2a that a larger number of singular values are important during the pulse than after the pulse, which is due to the fact that the populations of the higher Σ states that are involved in the transient dynamics during the pulse are going back to zero when it is over. Figure 2b shows how much of the trace of the density matrix, $\mathrm{Tr}\left[\rho_{mol}^{m}(t)\right]$ (Eq.(9)) is recovered for an increasing number of singular values, σ_m, *m*= 1 to 5. Five singular values suffice to recover the trace of the density matrix of the ensemble of 800 randomly oriented molecules with a precision better than of 10^{-3} during the pulse and of 10^{-5} after it is over, see Figure 3a. In figure 3b, we plot on a log scale the set of the 25 largest singular values at the maximum of the pulse (12.3 fs) and after the pulse, when the Hamiltonian and therefore the singular values are stationary (18 fs). One can see that indeed a 6th singular value would be needed to get an accuracy of 10^{-5} during the pulse. Figure 3b also shows that with 15 eigenvalues, the SVD fit reaches error values of $\approx 10^{-13}$ (numerically zero) which corresponds to the accuracy of the numerical integration of the TDSE.

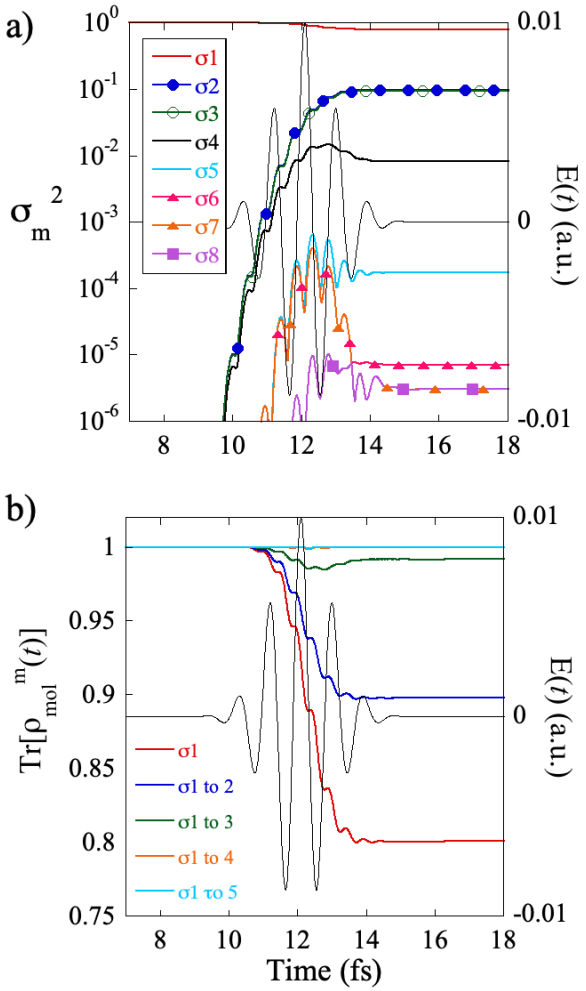

Figure 2. a) The time evolution of the 8 largest normalized singular values, σ_m^2 / N_0, during and after the pulse. The singular values of that correspond to molecular singular vectors $\mathbf{U_m}$ localized on the two components of Π states are plotted with markers so as to better identify them. The two pairs of degenerate singular values localize on the Π states, σ_2 and σ_3 on Π_1 (blue diamonds for Π_{1x} and green ones for Π_{1y}) and σ_6 (red triangles) and σ_7 (orange filled triangles) during the pulse and σ_7 and σ_8 (filled squares) after the pulse on Π_2. b) the cumulative trace recovered with an increasing number of singular values, from 1 to 5.

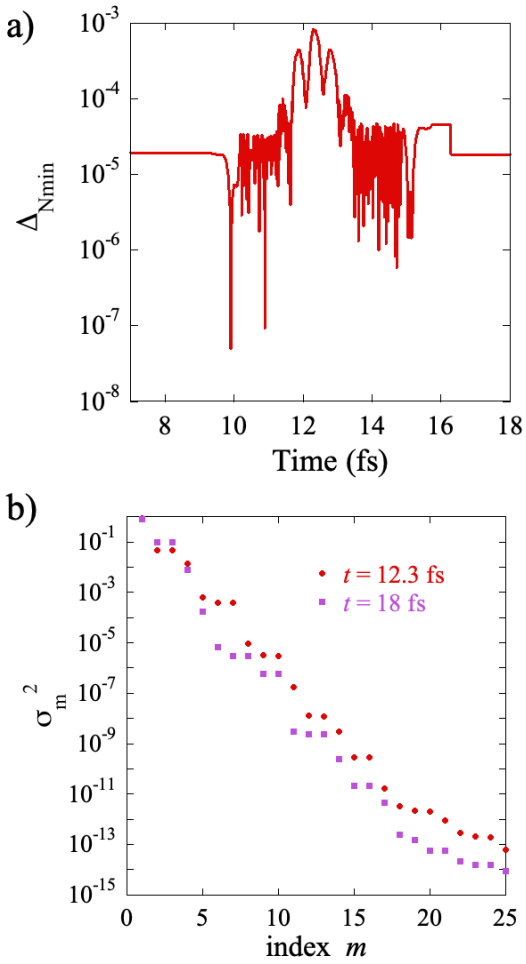

Figure 3: a) $\Delta_{N\min}$ (Eq. (9)) the absolute value on the error on the trace computed by including 5 singular values in the trace of the density matrix, $\mathrm{Tr}\left[\rho_{mol}^{5}(t)\right]$. b) the 25 largest normalized singular values computed at the maximum of the pulse (violet squares) and after the pulse, when their values are constant (red dots) at 18 fs. The doublets of degenerate singular values correlate with the two components of the Π states.

In figure 4, we show the localization of the molecular (left) singular vectors, $\mathbf{U_m}$, on the electronic states and along the R coordinate, at 18fs, after the pulse is over. $\mathbf{U_1}$, which corresponds to the largest singular value, is localized on the ground electronic state and corresponds to the ground vibrational state (the initial state). $\mathbf{U_2}$ and $\mathbf{U_3}$ are localized on the Π_1 state (on the y and x components respectively) with essentially equal values of σ_2 and σ_3. $\mathbf{U_4}$ is localized on the manifold of excited Σ states ($\Sigma_1, \Sigma_2, \Sigma_3, \Sigma_4$) with a σ_4 value an order

of magnitude smaller than σ_2 and σ_3. **U5** is localized on the GS but corresponds to excited vibrational states, with an even smaller value of σ_5.

The corresponding singular orientation vectors are shown in figure 5. **V1** (panel a) is distributed uniformly on the sphere, corresponding to the initial distribution of orientations, in agreement with the localization of **U1** on v =0 of the ground electronic state (see Figure 4). **V2** (panel c) and **V3** (panel d) are localized along the y and the x axis respectively since **U2** and **U3** are localized in the y and x components of the Π_1 state. **V4** (panel b) is localized along the z axis since it corresponds to excited Σ states. **V5** (figure S5) is a much smaller component and corresponds to excited vibrational state of the GS and is localized on z. We therefore see that the localization of the singular vectors is dictated by the symmetry the electronic states, which is conserved after the pulse since the NAC terms can only couple states of the same symmetry.

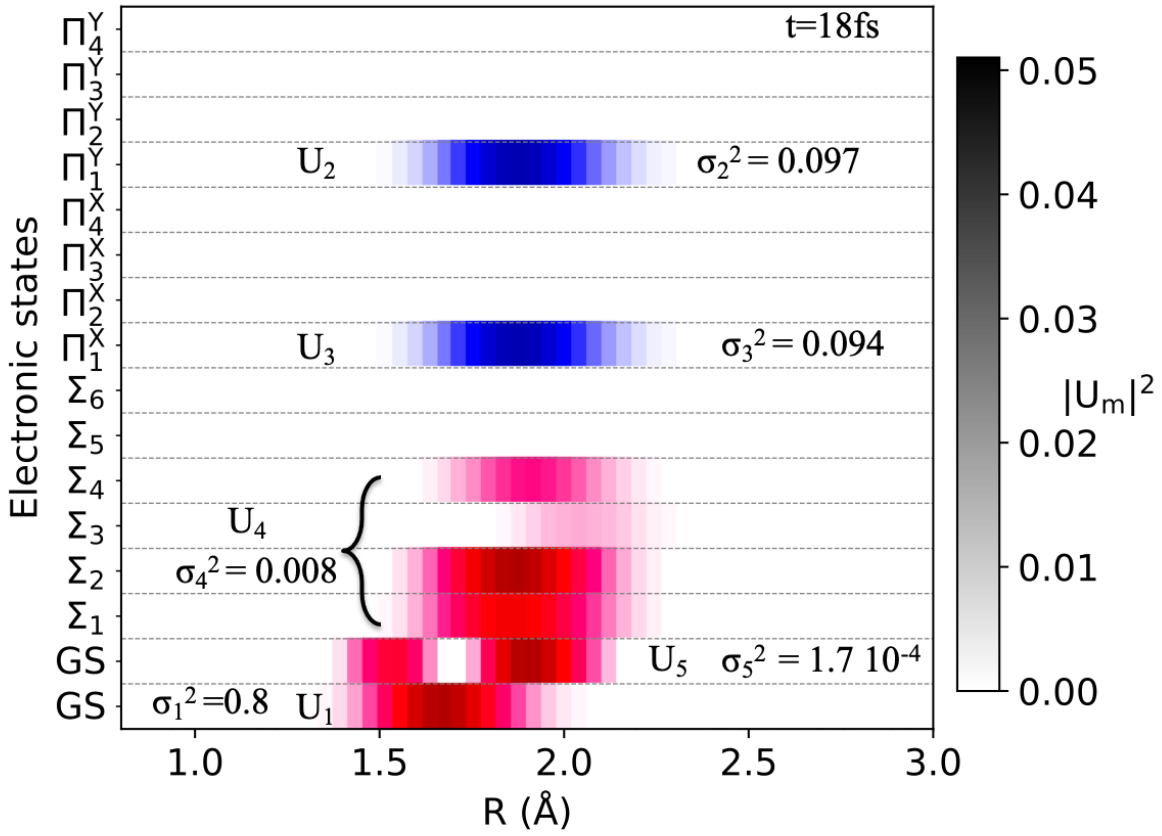

Figure 4: Localization of the molecular singular vectors **Um** on the grid for the 5 largest singular values. Computed for the excitation by the 2fs 4.35 eV pulse.

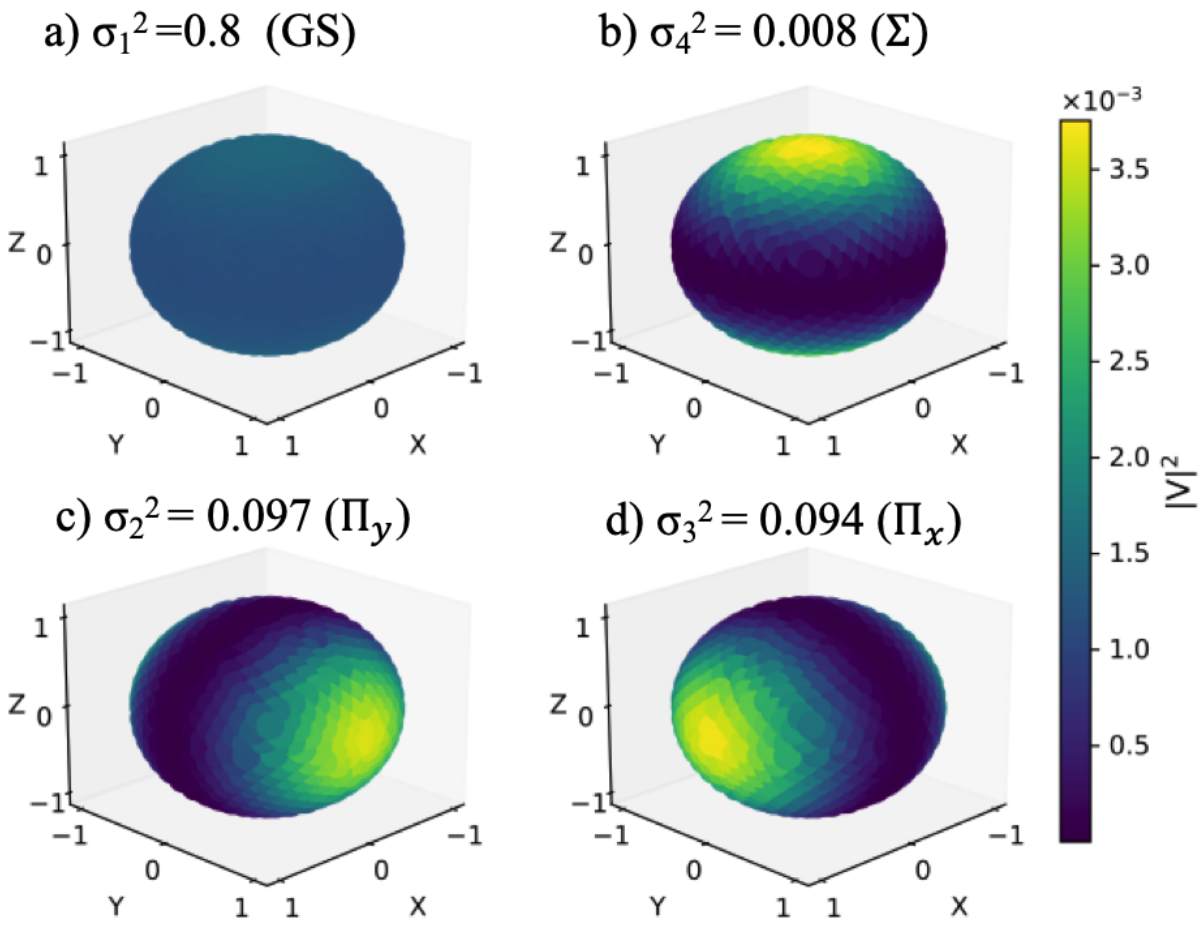

Figure 5: Orientation distribution on the unit sphere of the square modulus of the **V** vectors of the 4 largest principal components. $\mathbf{V_1}$ (panel a)is uniformly distributed over all orientations. $\mathbf{V_2}$ (panel c) and $\mathbf{V_3}$ (panel d) are oriented along y and x respectively to account for the excitation of the Π states while $\mathbf{V_4}$ (panel b) is oriented along z and accounts for the excitation of the Σ excited states. The colors code on the rhs is common to $\mathbf{V_2}$, $\mathbf{V_3}$ and $\mathbf{V_4}$. The V vectors are normalized to 1. $\mathbf{V_5}$, that is oriented along z as well, which corresponds to a more minor principal component. It shown in Figure S5.

Since the Hamiltonian is stationary after the pulse, the left eigenvectors, $\mathbf{U_m}$, which are localized on the grid and on the electronic states, can be used to compute the quantum dynamics of the ensemble. We do so using Eq. (10) by propagating numerically the 5 $\mathbf{U_m}$ vectors that correspond to the five largest singular values, σ_m, starting at the end of the pulse, 18 fs. Since the numerical precision of the integration is of the order of 10^{-12} for the 200 fs of the propagation time, the error that we make by retaining the 5 largest principal components (10^{-5} relative error on the trace of the density matrix $\rho_{mol}(t)$) does not increase. In parallel, as a

benchmark, we propagated the 800 initial states separately for 200 fs using the TDSE and the performed the averaging over these 800 $\left|\Psi_o(t)\right\rangle$.

The agreement between the two computations is excellent for the populations of electronic states, electronic coherences and for observables such as the time-dependent dipole moment, which depends on both the population and the coherences between electronic states and grid points. This is true not only for the states with a large population, like the two components of the Π_1 state and the GS plotted in Figure 1a, but also for the populations of the Σ states (Figure 1b), which have populations of a few tenths of percent only. The relative error for the population of the GS and of the Π_1 state computed as an exact average over the 800 orientations or by the SVD propagation of the 5 largest principal components is of the order 10^{-4} percent (Figure 6a), which can be understood from the fact that 4 among the 5 principal values retained for the SVD propagation localize on these states. For the manifold of Σ_1, Σ_2, Σ_3 and Σ_4 (Figure 6b), the error is larger, of the order of a tenth of percent, which again can be understood from the fact that the population in those states is only ≈ 100 times larger than the threshold (10^{-5}) fixed to recover the trace of the ensemble density matrix and that only one singular component, the fourth one, accounts for the dynamics of the populations in the excited Σ manifold. The largest error is made when the non adiabatic coupling is strong between the excited Σ states. For completeness, we show in Figure S6 that the populations computed by the two methods cannot be distinguished to reading accuracy.

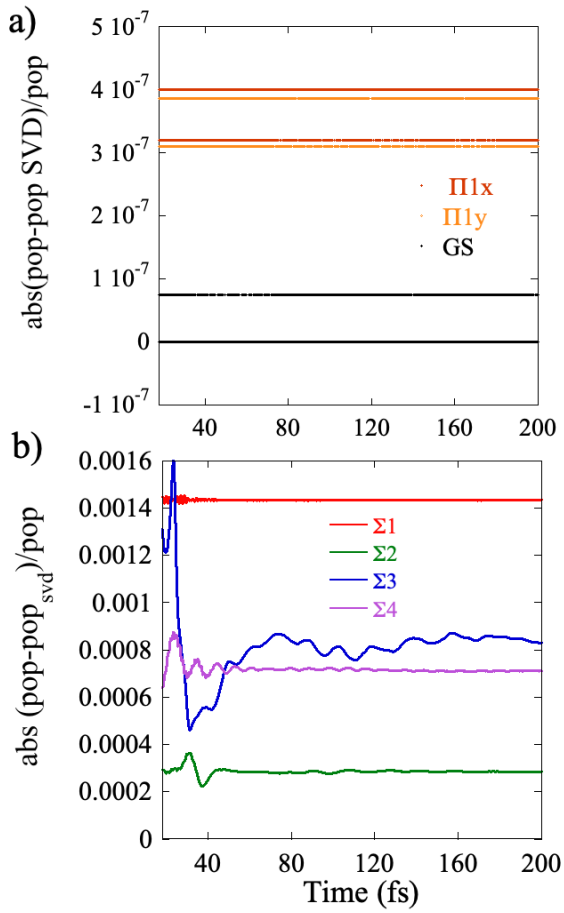

Figure 6. Relative errors on the populations of the GS and Π_1 states computed as an exact averaging over 800 initial orientations or by propagating the $\mathbf{U_m}$ vectors of the 5 largest principal components. The plot of the populations is shown in Figure S6. Figure S7 of the SI shows the error on the populations at 18 fs computed for 5, 8 ,10, 12 and 15 σ_m respectively.

In figure 7a, we show the full time-dependent dipole, $\mu(t)$, which is an observable very sensitive to the electronic and vibrational coherences. The fast ≈ 1 fs periods are the beatings between the Π_1 state and the GS while the longer beatings with a ≈ 10 fs period are between the Π_1 and the excited Σ states. Note that the amplitudes of $\mu(t)$ decreases in time because the GS and Σ_1 are bound, all the other excited states, including Π_1 are dissociative. The relative error for an increasing number of principal components taken into account in the dynamics is plotted in Figure 7b. One can see that 5 principal components give an relative error of 10^{-5}-10^{-4}, similar to that computed for the populations of the electronic states while already for 10 components, an error of 10^{-8} is reached. As for the populations, the largest error is made in the first 50 fs when the NAC between the Σ states is strong.

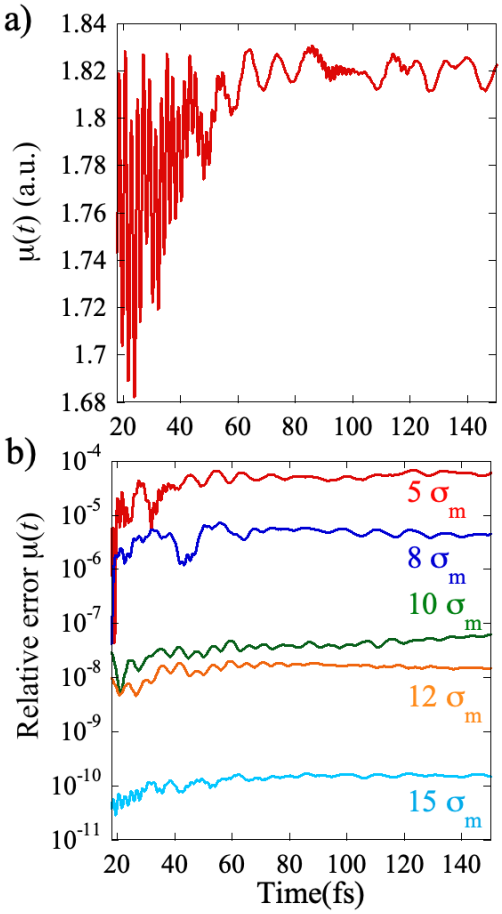

Figure 7. a) Full dipole moment, $\mu(t)$, computed for the exact averaging over 800 random orientation for the exciting 2fs deep UV (4.35 eV) pulse. b) relative error on $\mu(t)$ computed for an increasing number of principal components as indicated.

The results reported in Figures 6, 7 and S6 and S7 show that one can accurately describe the dynamics of the ensemble after the pulse is over by solving numerically the TDSE for the 5 molecular singular vectors, $\mathbf{U_m}$, instead of the 800 needed for an averaging over the initial random orientations. This represent a considerable saving of computer time and storage. One only need to propagate and store these 800 random oriented initial vectors during the pulse, for a dozen of femtosecond or so. The accuracy of the SVD propagation can be set by fixing a threshold for the recovery. For a threshold of the order of the accuracy of the numerical integration of the TDSE, one get essentially 'exact' results, as seen already for Figure 7. Setting a larger threshold inevitably introduces errors in the populations of the electronic states that are very small after the pulse is over, like the very low populations of the Σ manifold shown in Fig. 1. Another measure of the error is to use the Frobenius distance between the 'exact' density matrix obtained from averaging over 800 random initial orientations and the one recovered by

propagating a small number of $\mathbf{U_m}$ vectors. The Frobenius distance provides a measure of the error for the entire density matrix, and not only for its diagonal matrix elements as is provided by the difference in the trace, $\Delta_{N\min}$ (Eq.(9)) . The Frobenius distance is plotted in figure S8 on a log scale at t = 18 fs for an increasing number of principal components. Its distance is of the same order of magnitude as $\Delta_{N\min}$ (Eq.(9)) (Figure 3a) and on the error of on time-dependent dipole, $\mu(t)$, (Figure 7) and decreases in a similar way with the number of principal components included to recover the density matrix.

The expansion in terms of principal components, Eq. (11), is exact when all the N_o principal components are included. Otherwise the SVD theorem[14] states that including more singular values in the expansion will improve the fit or, at worst, not change it. Therefore, in the absence of a benchmark as for the example discussed above, one can readily determine the desired accuracy threshold by increasing the number of singular components used for propagating the TSDE after the pulse, based on the analysis of the values of the singular values and the error on the trace of the ensemble (Figures 4, 5 and S8) at the end of the pulse, here at 18 fs.

To illustrate further the power of the method, we now discuss the results for a second exciting pulse, with a slightly higher carrier frequency, (5.17 eV) so that the higher Σ and Π states are accessed with similar weights. In this case we only ran the dynamics for the 800 initial random molecular orientations until 18 fs, when the pulse is over. After the pulse is over, the propagation was carried out by integrating the TDSE using a few principal components, $\mathbf{U_m}$ vectors, Eq. ((10)).

We illustrate the convergence process of using an increasing number of principal components for the propagation of the pulse after 18 fs. We show in figure 8 the normalized singular values, σ_m^2, and the error on the trace of the ensemble as a function of the index m. We can distinguish two breaks in the magnitude of the singular values, one between m=4 and m=5 and one between m=8 and m=9. The same break is obtained for the Frobenius distance shown in Figure S8. The relative error, $\Delta_{N\min}$ Eq. (9) on the populations of the electronic states at 18fs is shown on figure 8b for 4 σ_m values.

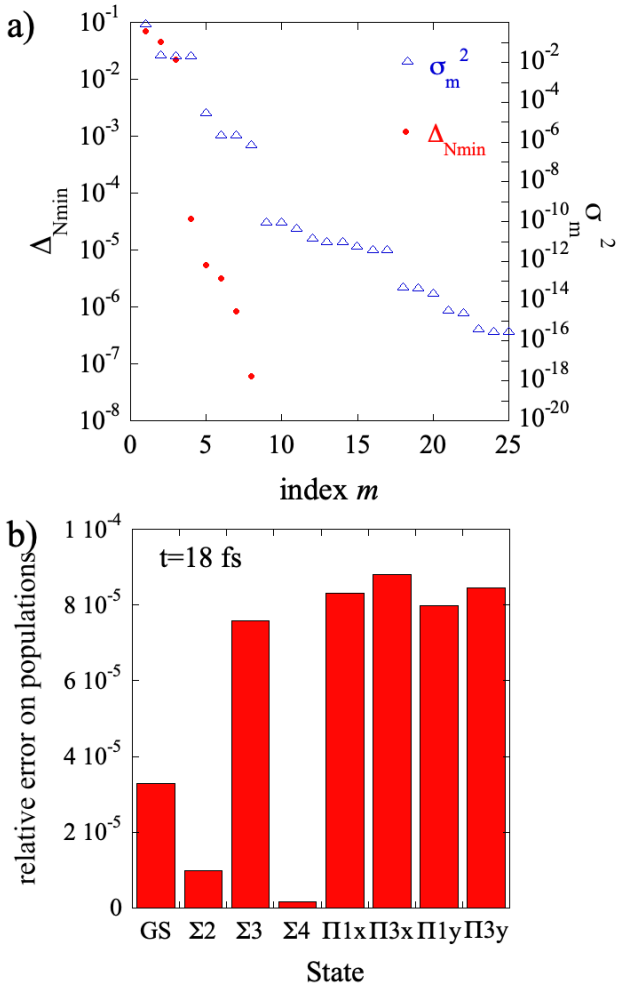

Figure 8. a) The normalized singular values, σ_m^2 , (right y axis) and $\Delta_{N\min}$ (right axis) at t =18 fs, computed for the excitation of LiH by a 2fs deep UV pulse with a carrier frequency of 5.17 eV and the error on the trace. b) Relative error on the populations computed for 4 σ_m.

The localization of the $\mathbf{U_m}$ vectors on the grid and on the electronic states at 18 fs is shown in Figure 9. $\mathbf{U_1}$ is localized on the GS, $\mathbf{U_2}$ on the manifold of excited Σ states, Σ_2, Σ_3 , Σ_4, and $\mathbf{U_3}$ and $\mathbf{U_4}$ on the x and y components of Π_1 and Π_3 respectively. Note how for this excitation, σ_2, σ_3 and σ_4 are essentially equal. Correspondingly, the $\mathbf{V_1}$ is uniform, $\mathbf{V_2}$ is localized along z, and $\mathbf{V_3}$ and $\mathbf{V_4}$ are localized along x and y respectively, see Figure S9.

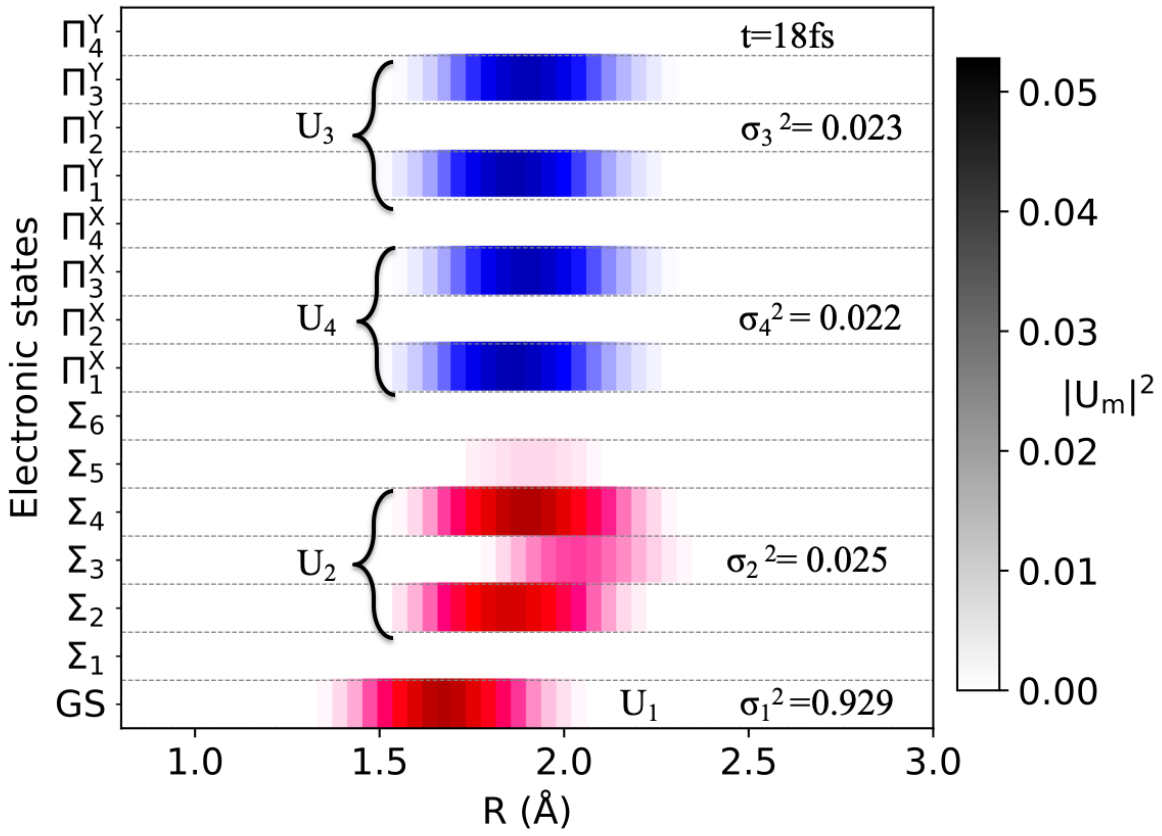

Figure 9: Heat map of the localization of the square modulus of the $\mathbf{U_m}$ vectors, m =1 to 4, for the dynamics induced by the 2fs deep UV (5.17 eV) pulse at t = 18fs, when the pulse is over.

The dynamics of the population transfer as well as the total dipole, computed by propagating the $\mathbf{U_m}$ vectors, are plotted in Figure 10 for 5 σ_m values and compared to the exact averaging over 800 orientations until 24 fs. We give in the figure 11 the differences between the values of the dipole computed for 5 σ_m, 10 σ_m and 15 σ_m. One can see that the value is essentially converged for 5 σ_m.

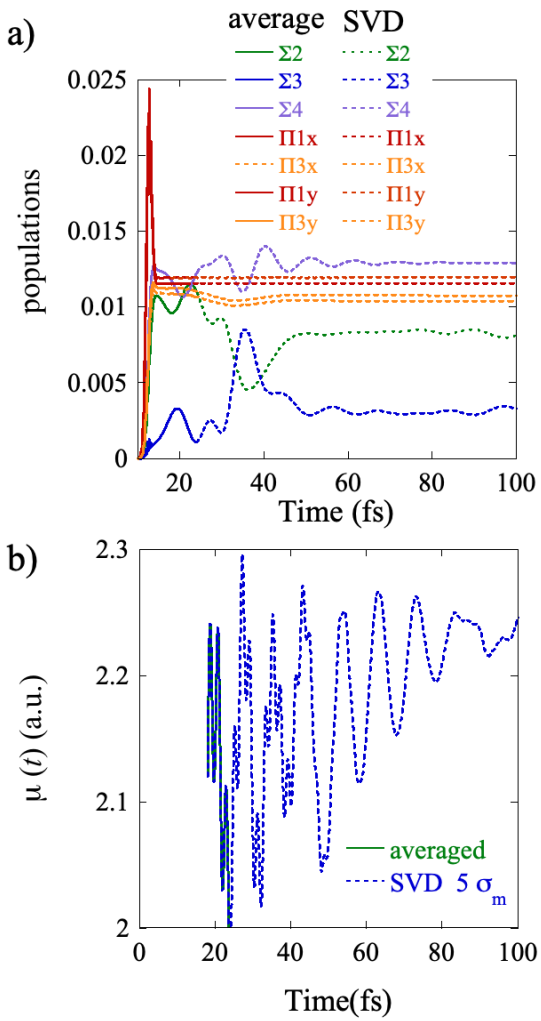

Figure 10. Populations (a) and time-dependent dipole, $\mu(t)$ (b), for the excitation by the 2fs deep UV 5.17 eV pulse. In panel a), the exact averaging over 800 initial random orientations is plotted in full lines up to 24fs. For later times, the approximate values computed by the propagation of 5 $\mathbf{U_m}$ vectors using the TDSE (Eq.(10)) is shown in dotted lines, starting at 18 fs. In Panel b) the same is done for the full time-dependent dipole, $\mu(t)$.

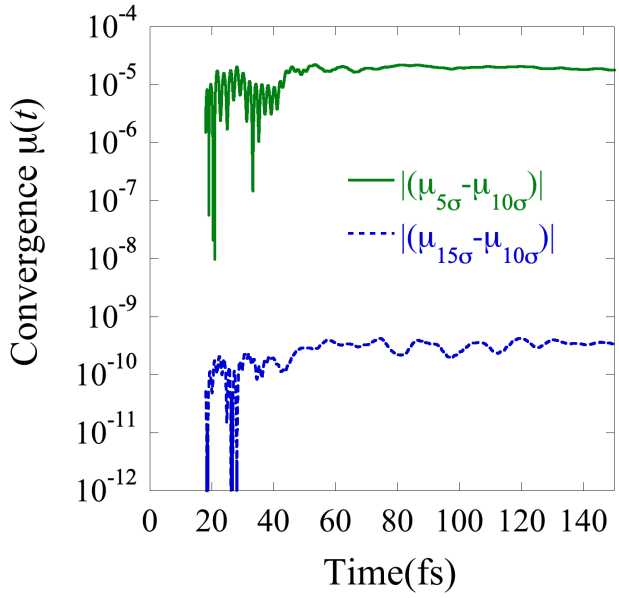

Figure 11. Convergence of the value of the time-dependent dipole, $\mu(t)$, for increasing number of principal components included in the propagation as indicated.

Conclusions

Our SVD based method allows for accurately describing the dynamics of the coherent excitation of an ensemble of randomly oriented molecules by a broad in energy ultrashort pulse that encompasses several electronic states. It shows that rather few singular vectors are sufficient to represent the ensemble of orientations of attosecond excited molecules which provides a storage and computer time efficient approach for studying the dynamics of coherently excited randomly oriented molecules. Equally noteworthy is that fewer than expected singular vectors are sufficient to represent the ensemble of excited electronic states. Even beyond that, note the stereodynamics: there is a one to one correspondence between the two sets of singular vectors. Each dominant orientation is thereby associated with its own coherent set of excited electronic states.

Acknowledgments

FR and MCG acknowledge the support of the Fonds National de la Recherche (F.R.S.-FNRS, Belgium), #T0205.20, and of the action of concerted research MECHANOCHEM (ARC 19/23-20, ULiege). Computational resources have been provided by the Consortium des Equipements de Calcul Intensif (CECI), funded by the F.R.S.-FNRS under Grant # 2.5020.11 The authors thanks the COST action ATTOCHEM (CA18222).

References

1. Vrakking, M. J. J.; Lepine, F., *Attosecond Molecular Dynamics*. The Royal Society of Chemistry: Cambridge, 2019; p P001-500.
2. Nisoli, M.; Decleva, P.; Calegari, F.; Palacios, A.; Martín, F., Attosecond Electron Dynamics in Molecules. *Chem. Rev.* **2017**, *117*, 10760-10825.
3. Remacle, F.; Levine, R. D., An Electronic Time Scale for Chemistry. *Proc. Natl. Acad. Sci. USA* **2006**, *103*, 6793-6798.
4. Remacle, F.; Nest, M.; Levine, R. D., Laser Steered Ultrafast Quantum Dynamics of Electrons in Lih. *Phys. Rev. Lett.* **2007**, *99*, 183902.
5. Stapelfeldt, H.; Seideman, T., Colloquium: Aligning Molecules with Strong Laser Pulses. *Rev. Mod. Phys.* **2003**, *75*, 543-557.
6. Gordon, R. J.; Zhu, L.; Seideman, T., Coherent Control of Chemical Reactions. *Acc. Chem. Res.* **1999**, *32*, 1007-1016.
7. Ghafur, O.; Rouzee, A.; Gijsbertsen, A.; Siu, W. K.; Stolte, S.; Vrakking, M. J. J., Impulsive Orientation and Alignment of Quantum-State-Selected No Molecules. *Nature Physics* **2009**, *5*, 289-293.
8. Kraus, P. M.; Baykusheva, D.; Wörner, H. J., Two-Pulse Field-Free Orientation Reveals Anisotropy of Molecular Shape Resonance. *Phys. Rev. Lett.* **2014**, *113*, 023001.
9. Fleischer, S.; Zhou, Y.; Field, R. W.; Nelson, K. A., Molecular Orientation and Alignment by Intense Single-Cycle Thz Pulses. *Phys. Rev. Lett.* **2011**, *107*, 163603.
10. Zare, R. N., *Angular Momentum, Understanding Spatial Aspects in Chemistry and Physics*; Wiley: New York, 1991.
11. Bernstein, R. B., *Chemical Dynamics Via Molecular Beam and Laser Techniques*; Oxford University Press: Oxford, 1992.
12. Bernstein, R. B.; Herschbach, D. R.; Levine, R. D., Dynamical Aspects of Stereochemistry. *J. Phys. Chem.* **1987**, *91*, 5365-5377.
13. Valentini, A.; van den Wildenberg, S.; Remacle, F., Selective Bond Formation Triggered by Short Optical Pulses: Quantum Dynamics of a Four-Center Ring Closure. *Phys. Chem. Chem. Phys.* **2020**, *22*, 22302-22313.
14. Golub, G. H.; Reinsch, C., Singular Value Decomposition and Least Squares Solutions. In *Linear Algebra*, Wilkinson, J. H.; Reinsch, C.; Bauer, F. L., Eds. Springer Berlin Heidelberg: Berlin, Heidelberg, 1971; pp 134-151.
15. Jaynes, E. T., Information Theory and Statistical Mechanics. Ii. *Phys. Rev.* **1957**, *108*, 171-190.
16. van den Wildenberg, S.; Mignolet, B.; Levine, R. D.; Remacle, F., Temporal and Spatially Resolved Imaging of the Correlated Nuclear-Electronic Dynamics and of the Ionized Photoelectron in a Coherently Electronically Highly Excited Vibrating Lih Molecule. *J. Chem. Phys.* **2019**, *151*, 134310.